Electronic Supplementary Material (ESI) for Journal of Materials Chemistry A.

Supporting Information

Nanostructured $BiVO_4$ obtained from vanadium calcination of nanohelixes Bi_2O_3 for enhanced photoelectrochemical water splitting

*Sucheol Ju,[a‡] Noho Lee,[b‡] Hansang Sung,[a‡] Soomin Son,[a] Nakhyun Kim,[a] Jaerim Kim,[b] Jong kyu Kim,[*b] and Heon Lee [*a,c]*

‡. Sucheol Ju, Noho Lee, and Hansang Sung contributed equally to this work.

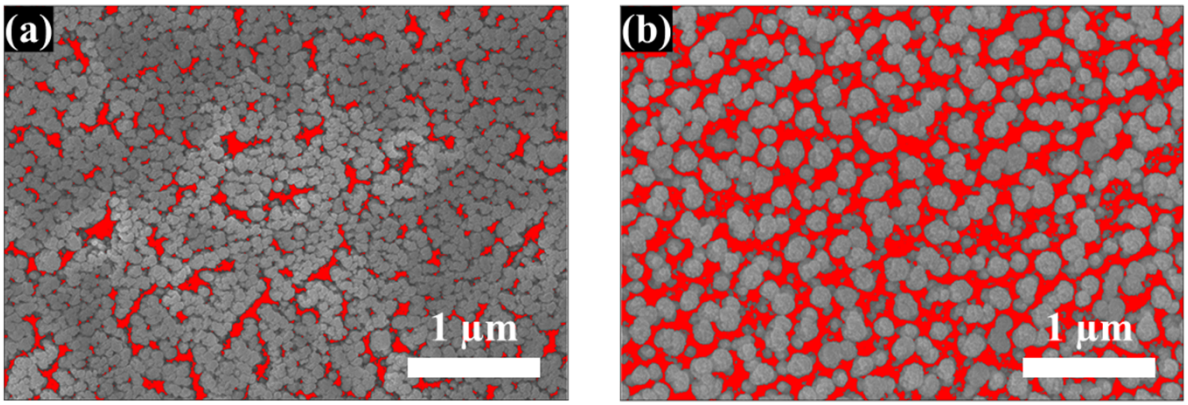

Figure S1. The calculation of the Bi_2O_3 nanohelix coverage using ImageJ software: (a) BO-80 and (b) BO-85.

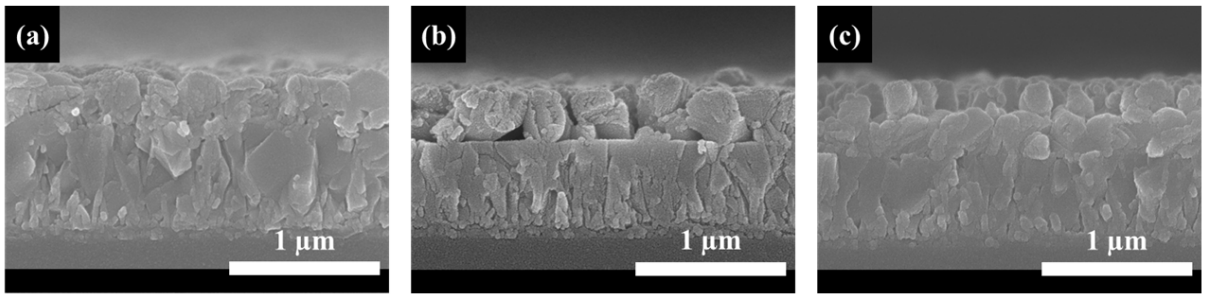

Figure S2. Scanning electron microscopy (SEM) images of (a) BVO-0, (b) BVO-80, and (c) BVO-85.

.

Table S1. Surface area and surface area ratio of BVO-0, BVO-80, and BVO-85 measured by atomic force microscopy (AFM; surface area of 9.0 μm^2).

	BVO-0	**BVO-80**	**BVO-85**
Surface area (μm^2)	10.9	12.0	19.9
Surface area ratio (%)	21.1	33.5	121.6

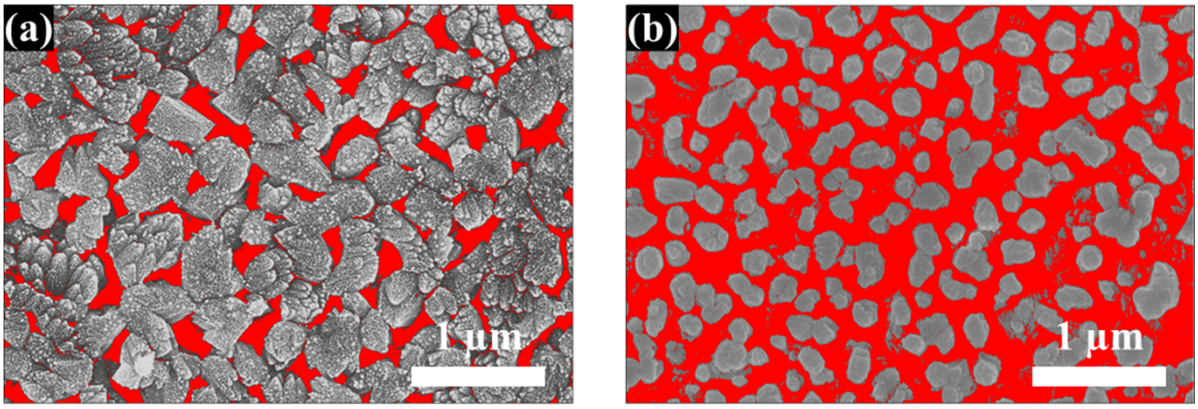

Figure S3. The calculation of the porosity using ImageJ software: (a) BVO-80 and (b) BVO-85.

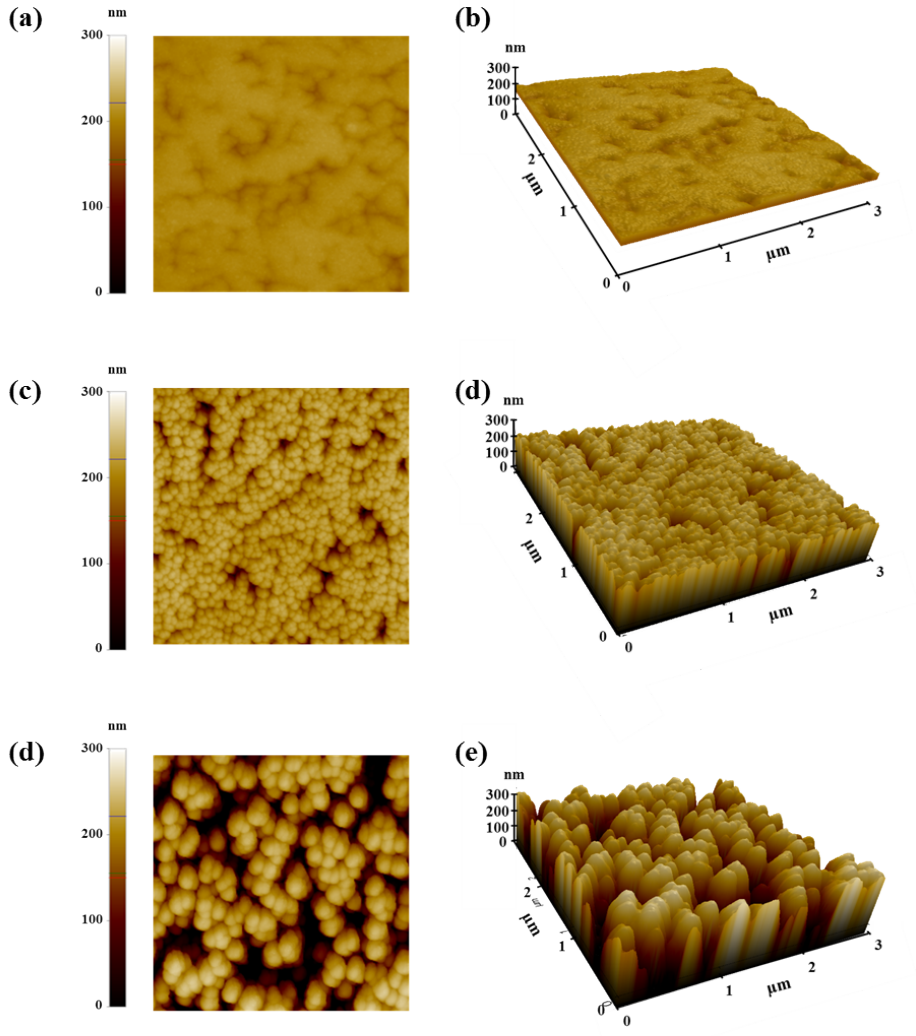

Figure S4. The respective two- and three-dimensional AFM images of (a, b) BO-0, (c, d) BO-80, and (d, e) BO-85.

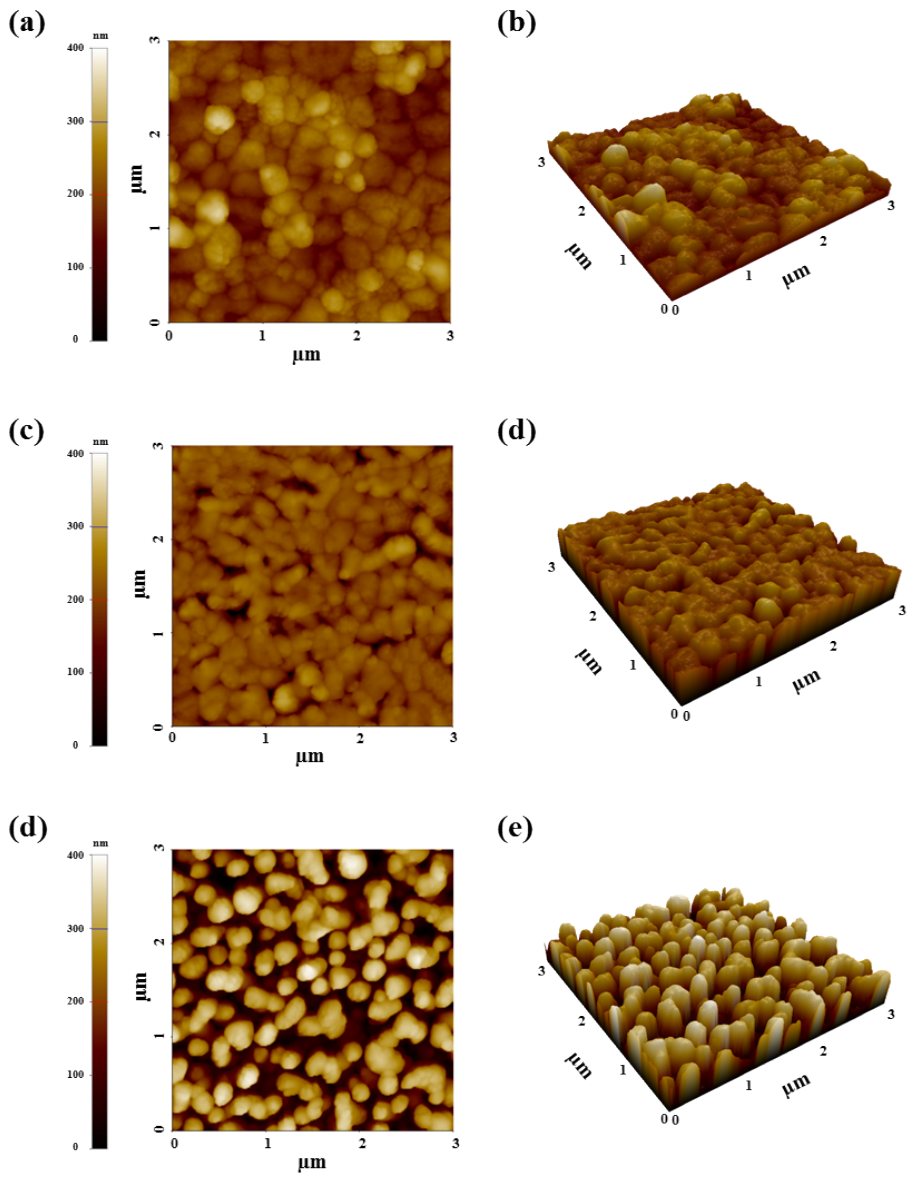

Figure S5. The respective two- and three-dimensional AFM images of (a, b) BVO-0, (c, d) BVO-80, and (d, e) BVO-85.

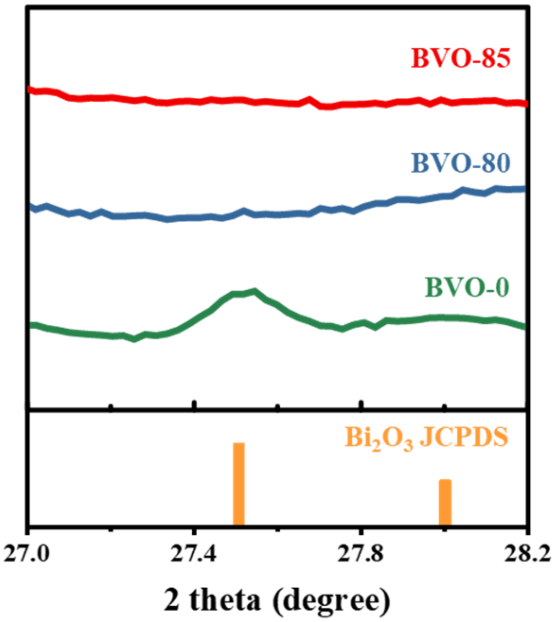

Figure S6. The narrow-scan X-ray diffraction (XRD) spectra of BVO-0, BVO-80, and BVO-85.

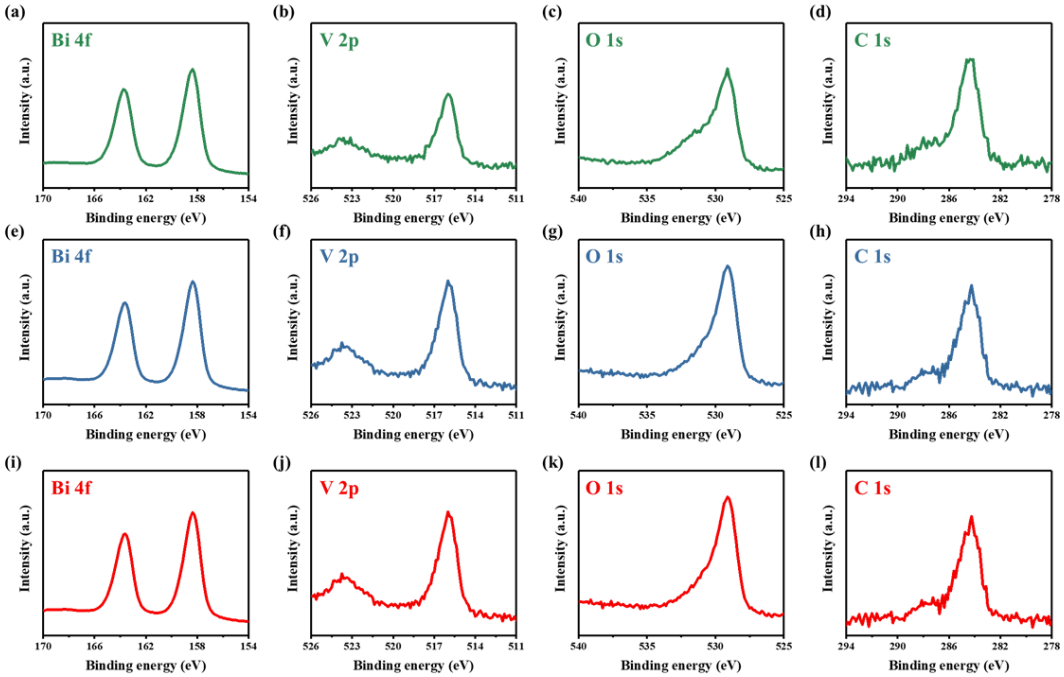

Figure S7. The narrow-scan X-ray photoelectron spectroscopy (XPS) results for (a–d) BVO-0, (e–h) BVO-80, and (i–l) BVO-85.

X-ray photoelectron spectroscopy was conducted to confirm the surface chemical states and compositions. Figures S4 presents the narrow-scan XPS spectra of Bi, V, and O for the three samples. The binding energies at 164.08 and 158.77 eV correspond to Bi $4f_{5/2}$ and $4f_{7/2}$ (Figures S4a, S4e, and S4i), respectively; whereas those at 524.08 and 516.25 eV correspond to V $2p_{1/2}$ and $2p_{3/2}$ (Figures S4b, S4f, and S4j), respectively. Figures S4c, S4g, and S4k present the binding energies of the oxygen vacancy (O_{vac}; 532.04 eV) and oxygen lattice (O_{latt}; 529.43 eV).

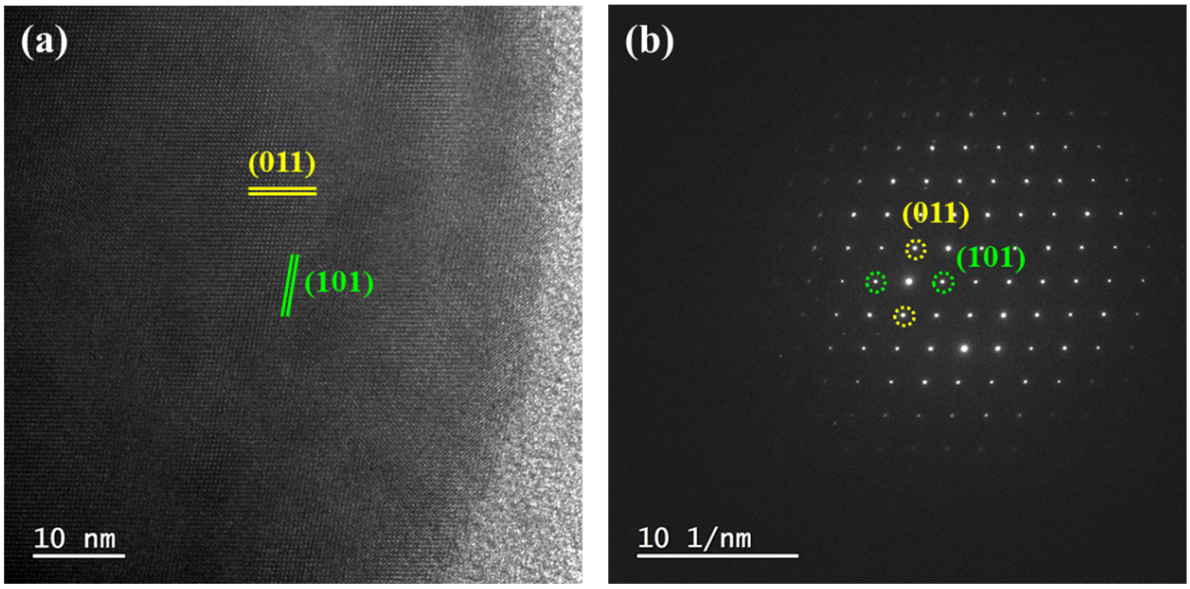

Figure S8. (a) High-resolution transmission electron image (TEM) and (b) fast Fourier transform (FFT) image of BVO.

The crystallinity of $BiVO_4$ was determined using transmission electron microscopy (TEM), as shown in Figure S5. The high-resolution TEM and FFT images present the monoclinic $BiVO_4$ lattice spaces of 0.474 and 0.493 nm, which correspond to the (011) and (101) facets, respectively.

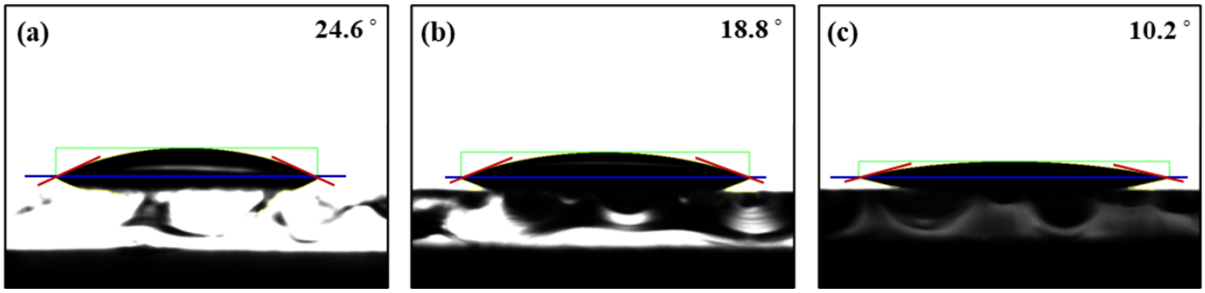

Figure S9. Contact angles between the V precursor and (a) BO-0, (b) BO-80, and (c) BO-85.

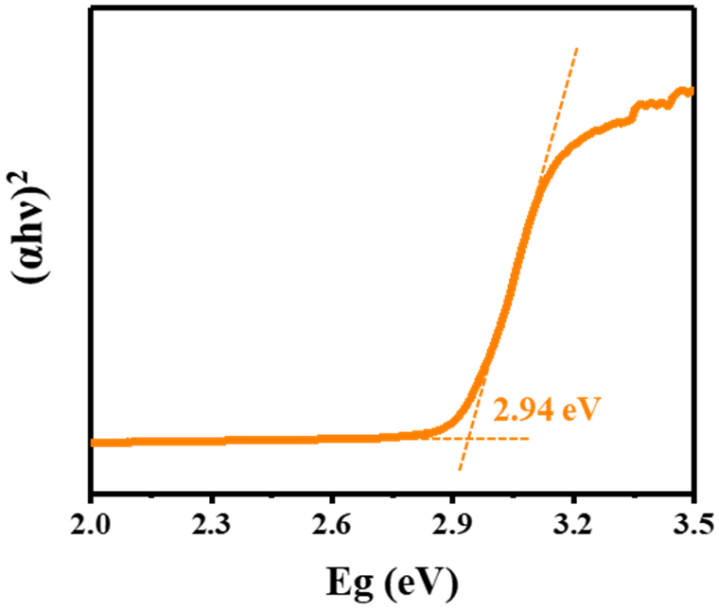

Figure S10. The Tauc plot for the deposited Bi_2O_3 based on UV–Vis spectroscopy.

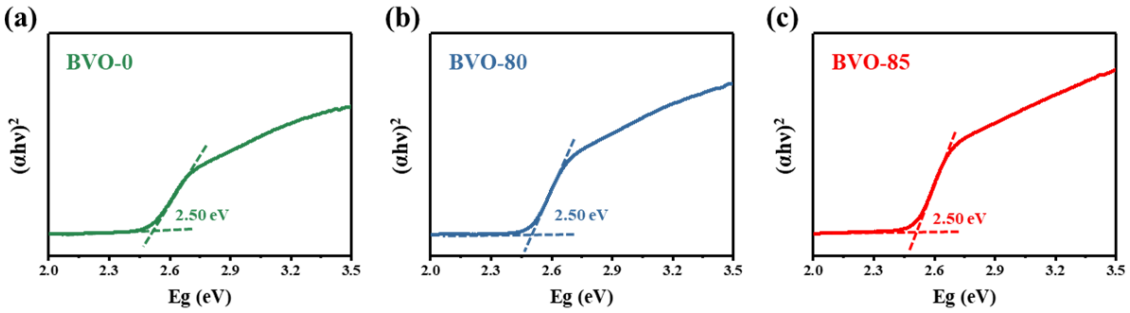

Figure S11. The Tauc plot for (a) BVO-0, (b) BVO-80, and (c) BVO-85 based on UV–Vis spectroscopy.

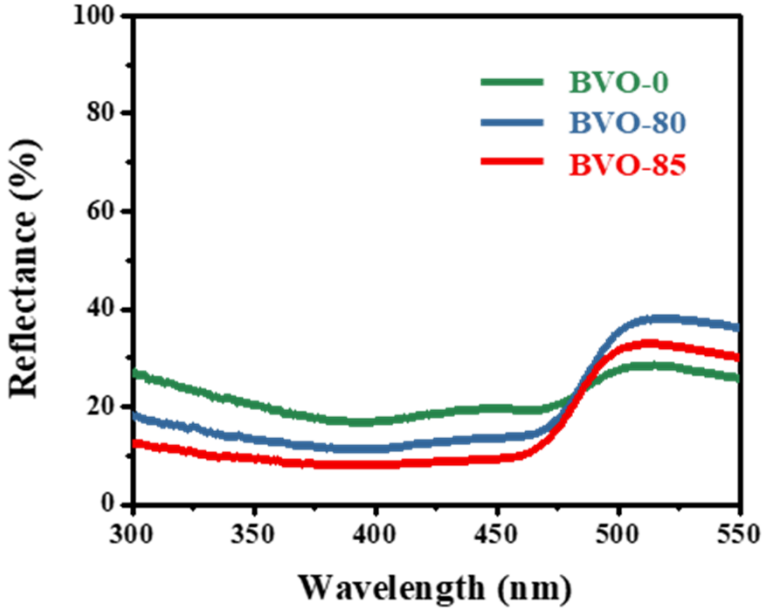

Figure S12. The reflectance graph of BVO-0, BVO-80, and BVO-85, as determined by UV–Vis with an integrating sphere.

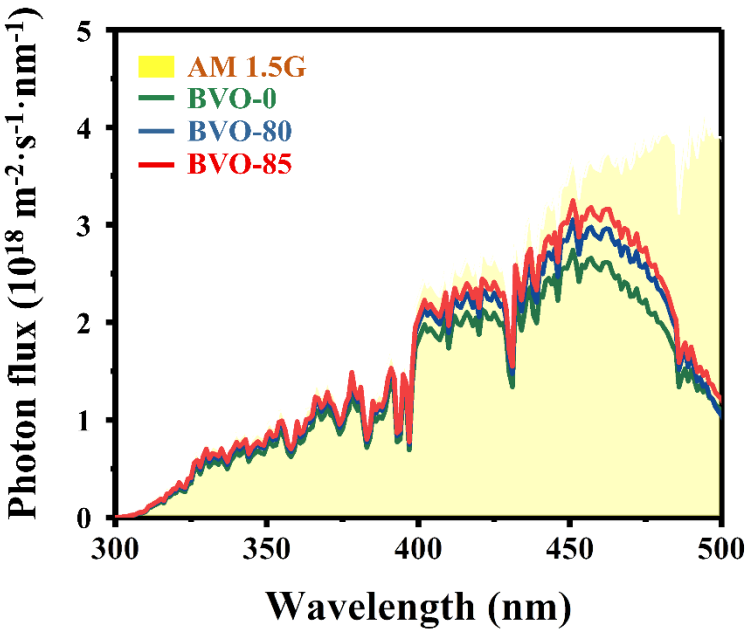

Figure S13. Photon flux of the AM 1.5 G solar spectrum, BVO-F, BVO-MP1, and BVO-MP2.

Table S2. The J_{abs} and η_{abs} values of BVO-0, BVO-80, and BVO-85

	BVO-0	**BVO-80**	**BVO-85**
$\boldsymbol{J_{abs}}$ (mA·cm^{-2})	4.29	4.76	5.01
$\boldsymbol{\eta_{abs}}$ (%)	69.2	76.7	80.8

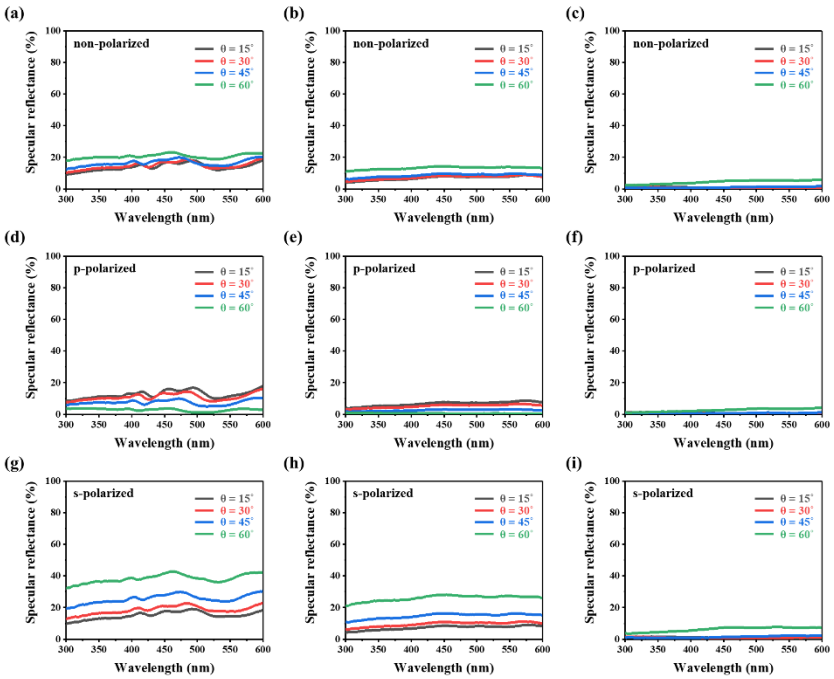

Figure S14. The non-polarized specular reflectance graph of (a) BVO-0, (b) BVO-80, and (c) BVO-85. The p-polarized specular reflectance graph of (d) BVO-0, (e) BVO-80, and (f) BVO-85. The s-polarized specular reflectance graph of (g) BVO-0, (h) BVO-80, (i) BVO-85.

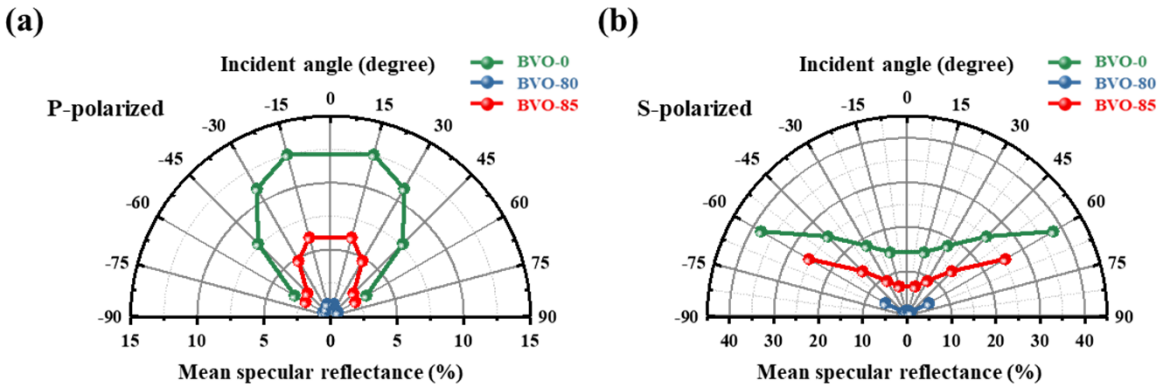

Figure S15. Mean angle-dependent specular reflectance of (a) p-polarized light and (b) s-polarized light for BVO-0, BVO-80, and BVO-85.

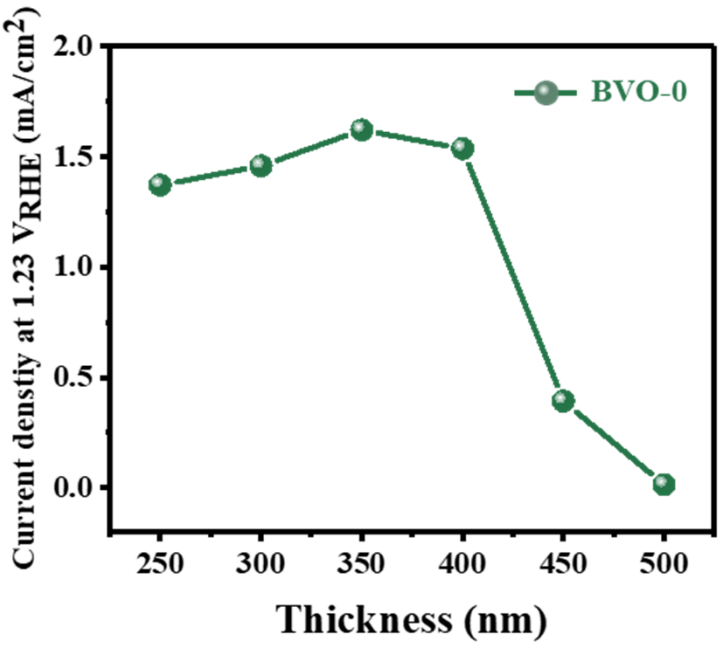

Figure S16. Current density of BVO-0 for difference thickness of $BiVO_4$ in a 0.5 M phosphate buffer solution under AM 1.5G illumination at 1.23 V_{RHE}.

Table S3. Comparison of the photocurrent densities with those of $BiVO_4$ photoanode studies fabricated by e-beam evaporation.

Reference	Structure	Fabrication method	Current density at 1.23 V_{RHE} (bare $BiVO_4$)
This work	Flat $BiVO_4$	Bi_2O_3 source deposited with e-beam evaporator and V calcination	1.61 mA/cm^2
This work	Nanostructured $BiVO_4$	Bi_2O_3 source oblique angle deposited with e-beam evaporator and V calcination	2.60 mA/cm^2
35	Flat $BiVO_4$	$BiVO_4$ source deposited with e-beam evaporator	~1 mA/cm^2
36	Nanostructured $BiVO_4$	$BiVO_4$ source deposited with e-beam evaporator	0.3 mA/cm^2

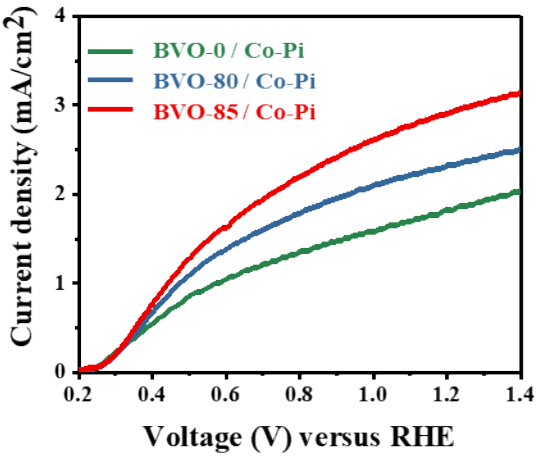

Figure S17. Linear sweep voltammetry (LSV) curve for BVO-0 / Co-Pi, BVO-80 / Co-Pi, / BVO-85 / Co-Pi measured in a 0.5 M phosphate buffer solution under 1-sun illumination.

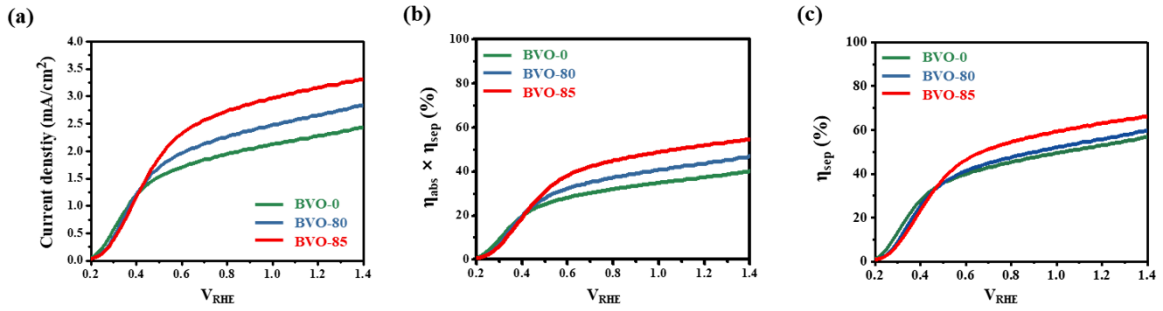

Figure S18. (a) Linear sweep voltammetry (LSV) curve measured in a 0.5 M phosphate buffer solution containing 0.5 M Na_2SO_3. Calculated values of (b) $\eta_{abs} \times \eta_{sep}$ and (c) η_{sep} for BVO-0, BVO-80, and BVO-85.

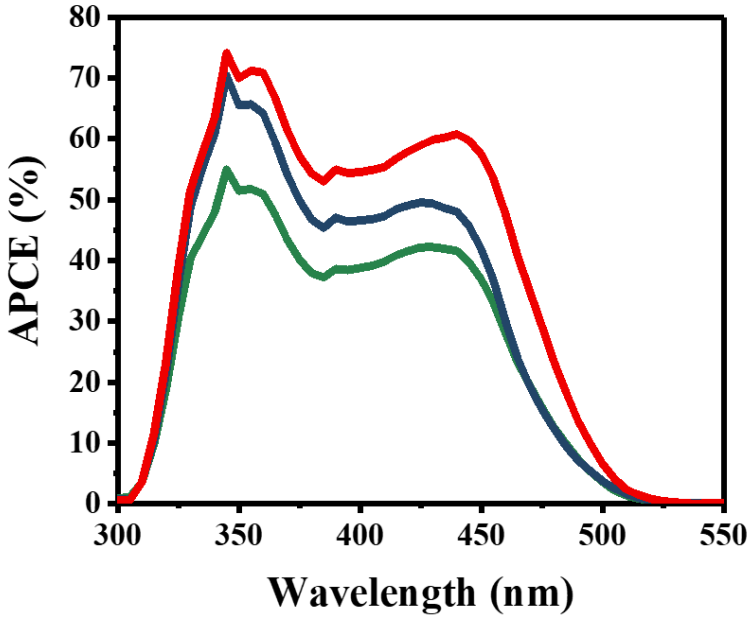

Figure S19. Absorbed photon-to-current efficiency (APCE) measured in a 0.5-M phosphate buffer solution at 1.23 V_{RHE}.

Table S4. Nyquist plot fitting results for BVO-0, BVO-80, and BVO-85

	BVO-0	**BVO-80**	**BVO-85**
R_s (Ω)	70.2	93.7	86.8
R_{ct} (Ω)	4800	4408	3252

Table S5. The calculated values of $\eta_{abs} \times \eta_{sep}$ and η_{sep} for BVO-0, BVO-80, and BVO-85.

	BVO-0	**BVO-80**	**BVO-85**
$\eta_{abs} \times \eta_{sep}$ (%)	37.1	43.4	51.4
η_{sep} (%)	53.6	56.5	63.7